Available online at www.sciencedirect.com
SCIENCE DIRECT®
Journal of Sound and Vibration 277 (2004) 987–1003
JOURNAL OF SOUND AND VIBRATION
www.elsevier.com/locate/jsvi

Sound attenuation in circular duct using slit-like short expansion of eccentric and/or serialized configuration

Akira Sadamoto[a,*], Yasuji Tsubakishita[b], Yoshinori Murakami[a]

[a] *Department of Mechanical Engineering, Tsukuba College of Technology, 4-3 Amakubo, Tsukuba, Ibaraki 305-0005, Japan*

[b] *Department of Mechanical Engineering, Chubu University, Kasugai, Aichi, Japan*

Received 22 October 2002; accepted 25 September 2003

Abstract

Sound attenuation in a circular duct is investigated by measurement and numerical calculation for using a slit-like short circular expansion chamber, termed 'slit' here, that performs as a resonator muffler in the duct. Since its resonant frequency depends on its depth, some depth-varying configurations of it are introduced in order to widen its effective frequency range. First, the performance of a set of serialized slits is examined. This configuration is composed by the slits located in series in the duct, having different diameters from each other and concentric to the duct. While this type of slit basically shows the summative performance of each composing slit, a certain interaction among slits occurs if the resonant frequency of each slit comes close to each other. Second, a single slit eccentric to the duct is examined. In every case of it treated here, two resonant frequencies are obtained. While the lower resonance seems to relate to the (1,0) mode in the slit, the higher one seems to relate to the corresponding concentric slit. Finally, a set of serialized slits eccentric to the duct is considered. Its property becomes considerably complicated against the two cases mentioned above. In certain configurations of it, however, a good performance for sound reduction is obtained.

1. Introduction

Properties of an acoustically short expansion chamber that performs as a resonator muffler in a duct have been studied by several researchers [1–3]. In our former research [4], the resonant characteristic of it was summarized comprehensively for a short circular expansion chamber concentric to a circular duct. One meaningful result of this research is that this resonant

*Corresponding author. Fax: +81-29-858-9372.
E-mail address: sada@a.tsukuba-tech.ac.jp (A. Sadamoto).

0022-460X/$ - see front matter © 2003 Elsevier Ltd. All rights reserved.
doi:10.1016/j.jsv.2003.09.028

phenomenon is maintained even if the length of the expansion becomes very short, as the expansion resembles a slit grooved on the duct wall. According to this appearance, hereafter, this short expansion is termed 'slit' for simplicity.

Since the slit is very short in the duct axial direction, it could be used practically as a simple and compact muffler. From this viewpoint, we also investigated the performance of a slit for noise reduction in actual machinery [5]. In this investigation, it was confirmed that the level of a discrete-frequency noise radiated form a centrifugal fan was reduced sufficiently using a slit attached on the inlet of the fan, when the resonant frequency of the slit coincided with the noise frequency.

The basic character of a slit is analogically interpreted as it performs like a side-branch muffler, whose effect for sound reduction is obtained at the resonant frequency of it. This frequency is determined by the condition that the length of the branch with an open-end correction length coincides with a quarter wavelength of the sound. This means that an effective frequency of a slit strongly depends on its depth (the difference between the slit and duct radius). Judging from this, if a certain modification was added to the slit for its depth, the characteristic of it could be changed intentionally. For example, if some slits having a different diameter from each other were located in series in a duct, the effective frequency range is expected to become wider. In this configuration, of course, it is favourable to keep the axial compactness in a certain extent. From another perspective, a single slit with circumferentially varying depth is expected to have a wider effective frequency range. This type of slit can be simply formed by a circular slit eccentric to the duct. As a similar configuration to this, Selamet et al. showed the property of a short expansion with an offset inlet and outlet [6,7]. The lowest l/d ratio they considered was 0.205 out of total 9 configurations they had studied spanning the range of $l/d = 0.205$–3.525, where l is the expansion length and d is its diameter. On the contrary, our interest is focused on the range of $l/d < 0.1$. If such a short expansion (a slit) was applied to a duct with a fluid flow and the positions of its inlet and outlet were not coaxial, the slit must act as a large disturbance for the flow because the flow path becomes very narrow at the slit. As far as the slit is concerned, therefore, the inlet and outlet ducts should be coaxial with each other, though flow effects are not considered in the present research.

In this paper, sound transmission properties at several types of slit as mentioned above and a mixed configuration of them are studied by experiment using a well-designed apparatus and by numerical calculation developed in a three-dimensional sound field and solved using finite difference method (FDM). In every case considered in this paper, the incident wave to the slit is limited to the plane wave, and the duct contains no mean flow.

2. Experimental apparatus

The outline of the experimental apparatus is shown in Fig. 1. It is composed to measure sound transmission properties of several types of expansion located between two steel pipes, whose inner diameters are fixed at $D = 41.3$ mm in this research. Each pipe has a flange at each opposite end. Between these two flanges, several steel rings with various inner diameter and thickness and/or eccentricity to the pipe axis are placed to form several expansions. Details of these expansions are indicated in Section 4.

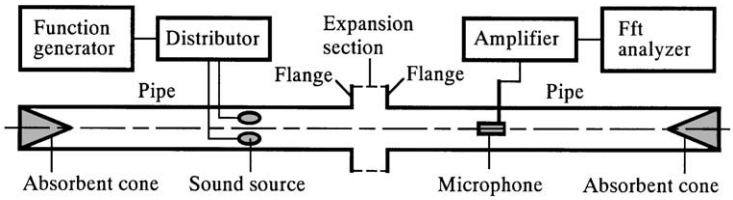

Fig. 1. Experimental apparatus.

The sound source consists of four small speakers (16 mm in diameter each) located in the pipe wall at intervals of 90° in the circumferential direction. The microphone (5.6 mm in diameter) is inserted in the pipe and traversable in the radial direction. Since the plane wave is considered in this research, it is required to radiate and receive the plane wave only. For this reason, each of four speakers radiates sinusoidal wave with the same frequency, amplitude and phase, and the microphone is fixed at the centre of the pipe cross-section.

The absorbent cones are used for avoiding the sound reflections at the ends. Naturally, their efficiency weakens in a certain low-frequency range. On the other hand, the performance of the speaker and microphone worsens in a certain high-frequency range, in which higher order modes becoming cut-on in the duct also makes the measurement difficult. From these reasons, the frequency range in Section 4 is limited to 2–7.5 kHz for keeping accuracy of the experiment. Although this frequency range seems rather high for practical applications, it matches some noises of actual machinery, e.g., a home-use vacuum cleaner's one [5]. In addition, for a simple linear acoustic field, any frequency can easily be normalized by the dimensions of the duct and slit, e.g., the frequency reduces to half when every size of the duct and slit doubles.

Using the apparatus in Fig. 1, sound transmission coefficient at the expansion section is obtained. This is the ratio of sound pressure amplitudes that are measured in the following two cases: (1) the case that the expansion of interest is composed between the two flanges and (2) the case that the expansion section is replaced with the ring that has the same inner diameter of the pipe and the same length of the expansion of interest, i.e., a simple straight pipe is composed between the sound source and the microphone.

Every measurement in this paper was conducted at the room temperature kept in 25 ± 1°C. In Section 4, hence, every calculation was carried out under the condition of 25°C, at which the sound speed in a free space becomes 346.75 m/s.

3. Calculation method

3.1. Basic equations

Several equations for a numerical analysis were developed for a three-dimensional sound field in a cylindrical duct with an expansion section as shown in Fig. 2, where the orthogonal co-ordinate system (x, y, z) is applied. The x-axis coincides with the duct axis and its origin is located at the centre of the expansion section.

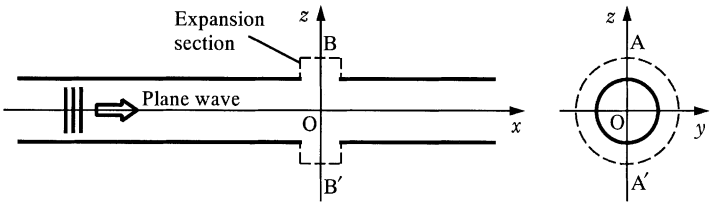

Fig. 2. Computational model.

The sound field is supposed to be governed by the linearized Euler equation, which becomes the system of equations for acoustic disturbance

$$\frac{\partial \mathbf{U}}{\partial t}+\frac{\partial \mathbf{E}}{\partial x}+\frac{\partial \mathbf{F}}{\partial y}+\frac{\partial \mathbf{G}}{\partial z}=\mathbf{H}, \tag{1}$$

where

$$\mathbf{U}=\begin{pmatrix}\rho'\\ \rho_0 u'\\ \rho_0 v'\\ \rho_0 w'\end{pmatrix},\quad \mathbf{E}=\begin{pmatrix}\rho_0 u'\\ p'\\ 0\\ 0\end{pmatrix},\quad \mathbf{F}=\begin{pmatrix}\rho_0 v'\\ 0\\ p'\\ 0\end{pmatrix},\quad \mathbf{G}=\begin{pmatrix}\rho_0 v'\\ 0\\ 0\\ p'\end{pmatrix}\quad \text{and}\quad \mathbf{H}=\begin{pmatrix}m\\ 0\\ 0\\ 0\end{pmatrix}, \tag{2}$$

$$p'=c_0^2\rho'\quad \text{and}\quad c_0=\sqrt{\gamma\frac{p_0}{\rho_0}}, \tag{3}$$

where subscript 0 denotes ambient quantity of the medium, prime denotes acoustic contribution, t is the time, ρ is the fluid density, p is the pressure, u, v and w are the velocities in the directions to x, y and z, respectively, γ is the ratio of specific heat and c is the sound speed.

In Eq. (2), the term m corresponds to the sound source composed by harmonic sink and source of mass to produce the plane wave in the duct

$$m=\frac{\rho_0 c_0}{D}\sin\omega t\cdot\delta(x-x_s)\quad \text{for } t\geqslant 0\quad \text{and}\quad m=0\quad \text{for } t<0, \tag{4}$$

where D is the duct diameter, $\omega=2\pi fD/c_0$, f is the frequency; and x_S is the location of the sound source. Delta function $\delta(x)$ is approximated using the Gauss function as

$$\delta(x)=\sqrt{\frac{\tau}{\pi}}\cdot\exp(-\tau x^2), \tag{5}$$

where $\tau=500$.

While the equations mentioned above are denoted by the xyz co-ordinate system, they are transformed and solved in an arbitrary-curved co-ordinate system (ξ,η,ζ) in practical calculations. Referring to Tannehill et al. [8], Eq. (1) is transformed into

$$\frac{\partial \mathbf{U}_1}{\partial t}+\frac{\partial \mathbf{E}_1}{\partial \xi}+\frac{\partial \mathbf{F}_1}{\partial \eta}+\frac{\partial \mathbf{G}_1}{\partial \zeta}=\mathbf{H}_1, \tag{6}$$

where

$$\mathbf{U}_1 = \mathbf{U}/\mathrm{J}, \quad \mathbf{E}_1 = (\mathbf{E}\xi_x + \mathbf{F}\xi_y + \mathbf{G}\xi_z)/\mathrm{J}, \quad \mathbf{F}_1 = (\mathbf{E}\eta_x + \mathbf{F}\eta_y + \mathbf{G}\eta_z)/\mathrm{J},$$
$$\mathbf{G}_1 = (\mathbf{E}\zeta_x + \mathbf{F}\zeta_y + \mathbf{G}\zeta_z)/\mathrm{J} \quad \text{and} \quad \mathbf{H}_1 = \mathbf{H}/\mathrm{J}, \tag{7}$$

J is the Jacobian of the transformation,

$$\begin{aligned}\mathrm{J} &= \frac{\partial(\xi,\eta,\zeta)}{\partial(x,y,z)} = \xi_x\eta_y\zeta_z + \xi_y\eta_z\zeta_x + \xi_z\eta_x\zeta_y - \xi_z\eta_y\zeta_x - \xi_y\eta_x\zeta_z - \xi_x\eta_z\zeta_y \\ &= 1/(x_\xi y_\eta z_\zeta + x_\eta y_\zeta z_\xi + x_\zeta y_\xi z_\eta - x_\zeta y_\eta z_\xi - x_\eta y_\xi z_\zeta - x_\xi y_\zeta z_\eta)\end{aligned} \tag{8}$$

and the metrics (ξ_x, η_x, etc.) can be realized by

$$\begin{pmatrix} \mathrm{d}\xi \\ \mathrm{d}\eta \\ \mathrm{d}\zeta \end{pmatrix} = \begin{pmatrix} \xi_x & \xi_y & \xi_z \\ \eta_x & \eta_y & \eta_z \\ \zeta_x & \zeta_y & \zeta_z \end{pmatrix} \begin{pmatrix} \mathrm{d}x \\ \mathrm{d}y \\ \mathrm{d}z \end{pmatrix} \quad \text{and} \quad \begin{pmatrix} \mathrm{d}x \\ \mathrm{d}y \\ \mathrm{d}z \end{pmatrix} = \begin{pmatrix} x_\xi & x_\eta & x_\zeta \\ y_\xi & y_\eta & y_\zeta \\ z_\xi & z_\eta & z_\zeta \end{pmatrix} \begin{pmatrix} \mathrm{d}\xi \\ \mathrm{d}\eta \\ \mathrm{d}\zeta \end{pmatrix}. \tag{9}$$

3.2. Boundary conditions

As shown in Fig. 3, at an arbitrary point A on a rigid wall of an arbitrary-curved surface where η is constant, the parameters u', v', w', ρ' and p' are determined as the boundary conditions. At the point A, the normal unit vector is indicated as $\mathbf{n}$, and the unit vectors to the ξ and ζ directions are denoted by $\mathbf{t}_\xi$ and $\mathbf{t}_\zeta$, respectively. These vectors are described using the metrics as follows:

$$\mathbf{n} = \frac{(\eta_x,\eta_y,\eta_z)}{\sqrt{\eta_x^2+\eta_y^2+\eta_z^2}}, \quad \mathbf{t}_\xi = \frac{(x_\xi,y_\xi,z_\xi)}{\sqrt{x_\xi^2+y_\xi^2+z_\xi^2}} \quad \text{and} \quad \mathbf{t}_\xi = \frac{(x_\zeta,y_\zeta,z_\zeta)}{\sqrt{x_\zeta^2+y_\zeta^2+z_\zeta^2}}. \tag{10}$$

First, the perturbed velocity $\mathbf{u}' = (u', v', w')$ is formulated. The condition that $\mathbf{u}'$ cannot pass through the wall is written as

$$\mathbf{n}\cdot\mathbf{u}' = \frac{\eta_x u' + \eta_y v' + \eta_z w'}{\sqrt{\eta_x^2+\eta_y^2+\eta_z^2}} = 0. \tag{11}$$

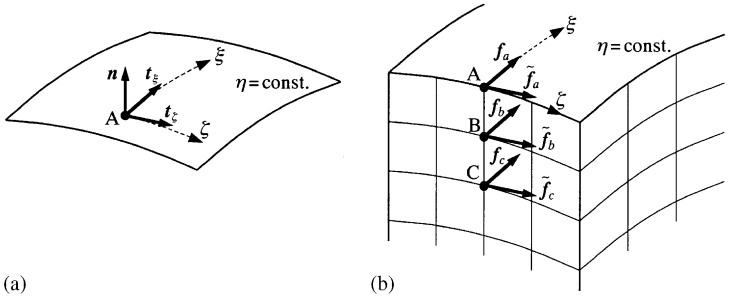

Fig. 3. Boundary conditions: (a) unit vectors on a rigid wall and (b) perturbed velocities.

On the other hand, $\mathbf{u}'$ flows along the wall to the ξ and ζ directions. Thus, the expressions of

$$\mathbf{t}_\xi \cdot \mathbf{u}' = \frac{x_\xi u' + y_\xi v' + z_\xi w'}{\sqrt{x_\xi^2 + y_\xi^2 + z_\xi^2}} = f_a \quad \text{and} \quad \mathbf{t}_\zeta \cdot \mathbf{u}' = \frac{x_\zeta u' + y_\zeta v' + z_\zeta w'}{\sqrt{x_\zeta^2 + y_\zeta^2 + z_\zeta^2}} = \tilde{f}_a \tag{12}$$

are adequate, where f_a is obtained by extrapolation using the velocity components f_b and f_c at the inner points B and C as shown in Fig. 3(b), and $\tilde{f}_a$ is obtained using $\tilde{f}_b$ and $\tilde{f}_c$ in the same manner. By solving Eqs. (11) and (12),

$$u' = \mathrm{J}[(z_\zeta \eta_y - y_\zeta \eta_z)\sqrt{x_\xi^2 + y_\xi^2 + z_\xi^2} f_a - (z_\xi \eta_y - y_\xi \eta_z)\sqrt{x_\zeta^2 + y_\zeta^2 + z_\zeta^2} \tilde{f}_a]/(\eta_x^2 + \eta_y^2 + \eta_z^2),$$

$$v' = \mathrm{J}[(x_\zeta \eta_z - z_\zeta \eta_x)\sqrt{x_\xi^2 + y_\xi^2 + z_\xi^2} f_a - (x_\xi \eta_z - z_\xi \eta_x)\sqrt{x_\zeta^2 + y_\zeta^2 + z_\zeta^2} \tilde{f}_a]/(\eta_x^2 + \eta_y^2 + \eta_z^2)$$

and

$$w' = \mathrm{J}[(y_\zeta \eta_x - x_\zeta \eta_y)\sqrt{x_\xi^2 + y_\xi^2 + z_\xi^2} f_a - (y_\xi \eta_x - x_\xi \eta_y)\sqrt{x_\zeta^2 + y_\zeta^2 + z_\zeta^2} \tilde{f}_a]/(\eta_x^2 + \eta_y^2 + \eta_z^2) \tag{13}$$

are obtained.

Second, equations for the sound pressure and the perturbed density on the wall (p' and ρ') are developed. Since the momentum equations in the xyz co-ordinate system are

$$\begin{aligned} M_1 &= \rho u_t + \rho(u u_x + v u_y + w u_z) + p_x = 0, \\ M_2 &= \rho v_t + \rho(u v_x + v v_y + w v_z) + p_y = 0 \\ M_3 &= \rho w_t + \rho(u w_x + v w_y + w w_z) + p_z = 0, \end{aligned} \tag{14}$$

the momentum equation in the perpendicular direction to the surface of $\eta = \text{const.}$ is

$$\mathbf{n} \cdot \mathbf{M} = \frac{\eta_x M_1 + \eta_y M_2 + \eta_z M_3}{\sqrt{\eta_x^2 + \eta_y^2 + \eta_z^2}} = 0, \tag{15}$$

which means there is no vector component of momentum normal to the surface of $\eta = \text{const}$ [9]. By substituting Eqs. (11) and (14) into Eq. (15) and neglecting terms of second order or higher,

$$p'_\xi(\xi_x \eta_x + \xi_y \eta_y + \xi_z \eta_z) + p'_\eta(\eta_x^2 + \eta_y^2 + \eta_z^2) + p'_\zeta(\zeta_x \eta_x + \zeta_y \eta_y + \zeta_z \eta_z) = 0 \tag{16}$$

is obtained. From Eqs. (3) and (16), p' and ρ' can be determined.

3.3. Computation

The computation is based on an explicit finite difference scheme of MacCormack type that has fourth order accuracy in space and second order accuracy in time. This scheme (known as the 2-4 scheme) by Gottlieb and Turkel [10] has been used successfully for many applications of aeroacoustics due to the ease of programming and use. However, this scheme requires many grid points per wavelength; e.g., 25 points per wavelength are said to be adequate for a reasonable solution with less dissipation and dispersion errors.

In the present numerical model, fortunately, the computation does not require large amount of grid points even for three-dimensional problem from the following reasons: the wavelength of the sound is not small compared with the duct diameter (41.3 mm), as the shortest wavelength is

about 50 mm for the highest frequency in Section 4 (7 kHz for the calculation); and the region of wave propagation is confined in the duct unlike an outward sound radiation problem. We adopted, hence, the 2–4 scheme instead of other accurate methods [11].

To be concrete, the typical grid system in our calculation is composed of $680 \times 18 \times 24$ points in the region far from the slit, since a coarse mesh spacing is available sufficiently in such a region with no artificial dumping term. On the other hand, the region near the slit is divided into about 10 000 points for giving 25 or more points per wavelength in the region of $-9 \leqslant x/D \leqslant 9$ and 50 or more points in the slit with uneven mesh spacing.

If the sound from the source reaches the end of the calculation domain, where sound reflection occurs, the reflected sound begins to disturb the sound field of interest. To avoid this, the calculation domain is extended in the region of $-110 \leqslant x/D \leqslant 110$, where the computation can be continued until the sound field of interest becomes steady before the reflection occurs.

The computation code was written by the authors, and a CFD post-processor software 'FIELDVIEW' by Intelligent Light was used for drawing contour maps of the sound pressure level shown in Section 4.

4. Effects of slit-like expansions on sound

4.1. Serialized slits concentric to the duct

Serialized concentric slits are shown in Fig. 4 where three slits S_1, S_2 and S_3 are placed in series in a duct. The diameters of them are d_1, d_2 and d_3, respectively. In this paper, the interval of slit $w = 1$ mm is fixed as thin as possible for axial compactness of this configuration, except an extra case shown in Fig. 6. Each of the three slits has the same length l for giving each slit the same effectiveness of sound attenuation.

Fig. 5 shows the transmission properties of the serialized concentric slits. The measured data denoted by each circular mark were obtained using the apparatus in Fig. 1 placing five steel rings between the flanges. As realized in Fig. 4, each of three rings having a circular hole with specified diameter (d_1, d_2, d_3, each) and thickness l was used for each slit, and two rings having a hole with 41.3 mm in diameter and 1 mm in thickness were used for the partitions of the slit.

In each case of $l = 2$ mm in Figs. 5(a)–(c), it is clear that three minimums are observed in each curve of transmission coefficient. By comparison with our former results [4], it is found that each frequency, at which each minimum is obtained, coincides with the resonant frequency of each slit

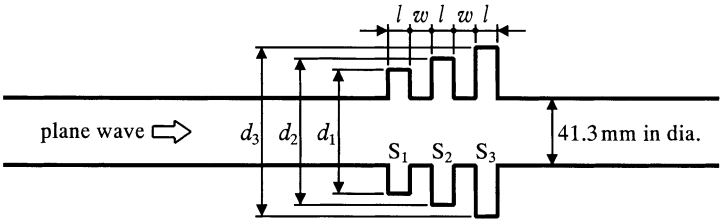

Fig. 4. Formation of serialized concentric slits.

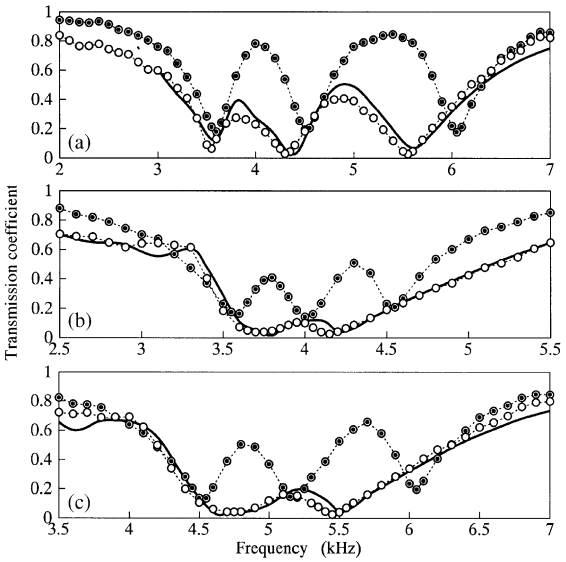

Fig. 5. Transmission coefficient at the serialized concentric slits, $D = 41.3$ mm, $w = 1$ mm: (a) $d_1 = 64$ mm, $d_2 = 72$ mm and $d_3 = 80$ mm; (b) $d_1 = 72$ mm, $d_2 = 76$ mm and $d_3 = 80$ mm; (c) $d_1 = 64$ mm, $d_2 = 68$ mm and $d_3 = 72$ mm; ◉, measured, $l = 2$ mm; ○, measured, $l = 5$ mm; ——, calculated by FDM, $l = 5$ mm.

(S_1, S_2 or S_3 in Fig. 4) that is individually placed in the duct. Therefore, it is reasonable to understand that the property of the serialized concentric slits is realized as showing the summative performance of each slit.

On the other hand, in Figs. 5(b) and (c), each curve of $l = 5$ mm does not have three minimums but has two minimums, and the frequencies of them come between the resonant frequencies of individually placed S_1, S_2 and S_3. This reduction of minimums might be caused by interaction of each slit, which is discussed later using Fig. 8.

In our former research [4], it was shown that the resonance effect of an individual slit strongly depends on l in the range of $l < 5$ mm, in which the minimum of transmission coefficient becomes larger and the dropping frequency range becomes narrower as l becoming shorter. This tendency is also seen in Fig. 5 by comparison of the curves of $l = 2$ and 5 mm.

Although $w = 1$ mm is fixed in Fig. 5 due to composing an axially compact muffler, it might be interesting to consider the effect of wider interval w. Fig. 6 shows the measured results in the same conditions of Fig. 5 with $l = 5$ mm but $w = 3$ mm ($w/l = 0.6$). In this figure, it is clear that each frequency of the minimums almost does not change from each one of $l = 5$ mm and $w = 1$ mm (Fig. 5, $w/l = 0.2$), and there is no indication of these frequencies approaching the ones of $l = 2$ mm in Fig. 5 ($w/l = 0.5$). It can be concluded, hence, the property of serialized slits more depends on the resonance effect of each composing slit than the interval of slit.

In order to confirm the influence of the arranging order of slit, the positions of the slits S_1 and S_3 were replaced with each other in Fig. 4. In this arrangement, the measured transmission coefficient was not changed at all in all the cases in Fig. 5.

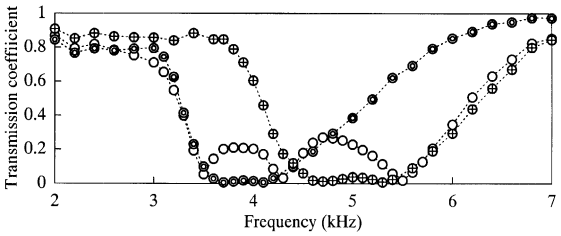

Fig. 6. Measured transmission coefficient at the serialized concentric slits, $D = 41.3\,\text{mm}$, $l = 5\,\text{mm}$, $w = 3\,\text{mm}$: ○, $d_1 = 64\,\text{mm}$, $d_2 = 72\,\text{mm}$ and $d_3 = 80\,\text{mm}$; ◎, $d_1 = 72\,\text{mm}$, $d_2 = 76\,\text{mm}$ and $d_3 = 80\,\text{mm}$; ⊕, $d_1 = 64\,\text{mm}$, $d_2 = 68\,\text{mm}$ and $d_3 = 72\,\text{mm}$.

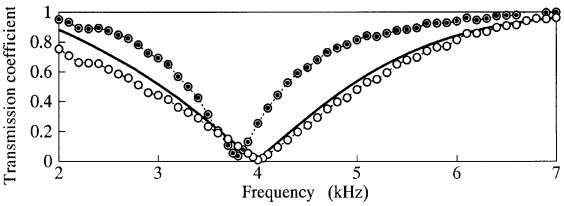

Fig. 7. Transmission coefficient at the stepped chamber, $D = 41.3\,\text{mm}$, $w = 0\,\text{mm}$, $d_1 = 72\,\text{mm}$, $d_2 = 76\,\text{mm}$ and $d_3 = 80\,\text{mm}$: ◎, measured, $l = 2\,\text{mm}$; ○, measured, $l = 5\,\text{mm}$; ——, calculated by FDM, $l = 5\,\text{mm}$.

For reference, Fig. 7 shows results for $w = 0$, i.e., the case that the three slits S_1, S_2 and S_3 are combined to form a single expansion with its outer diameter varying stepwise. In this case, the number of the minimums of the curve becomes one. By comparison with the result of our former research [4], it is found that the transmission coefficient of this stepped expansion completely coincides with the one of the simple expansion with diameter d_2 (76 mm) and length $3l$ (6 mm for $l = 2\,\text{mm}$, 15 mm for $l = 5\,\text{mm}$). Hence, there is no meaning to compose such a stepped expansion for sound reduction's sake.

In Figs. 5 and 7, each thick solid curved-line shows the calculated result for $l = 5\,\text{mm}$ obtained by the FDM computation. The calculated transmission coefficient is determined by the same manner as the experiment, i.e., it is obtained as the ratio of sound pressure amplitude at the duct axis. Since the agreements between the measured and calculated results are good in these figures, the FDM calculation based on the formulation in Section 3 is applicable to consideration of sound field in the duct shown in Fig. 4.

Fig. 8 shows several distributions of sound pressure level in the duct with the three slits of $l = 5\,\text{mm}$. Each contour map corresponds to each resonance in Figs. 5(a) and (b), and shows the upper half cross-section of AA′ in Fig. 2, i.e., the bottom line of each map corresponds to the duct axis. For the sound pressure level in this figure, the reference level is 126 dB at the sound source in the duct with no slits. This reference level also applies to Figs. 13 and 16 in the following sections.

In each contour map in Fig. 8, it is clear that a standing wave is composed in the left hand duct (incident side) caused by interaction between the incident and reflected wave. In contrast, the level becomes low and almost uniform in the right hand duct (transmitted side). In and near the slits, the distribution apparently differs from one map to another.

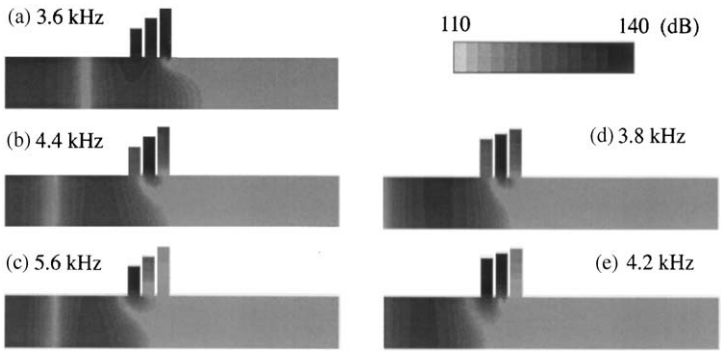

Fig. 8. Distribution of sound pressure level in the duct with the serialized concentric slits, $D = 41.3$ mm, $w = 1$ mm, $l = 5$ mm: (a)–(c), $d_1 = 64$ mm, $d_2 = 72$ mm and $d_3 = 80$ mm; (d) and (e), $d_1 = 72$ mm, $d_2 = 76$ mm and $d_3 = 80$ mm.

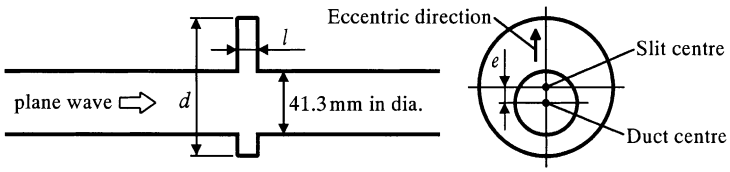

Fig. 9. Formation of a single eccentric slit.

In Figs. 8(a)–(c), the highest level of each case is observed in the slit corresponding each resonance, in other words, each one of the three slits becomes dominant at each resonant frequency. In addition, the region of node that has lower level relative to the ambient level and connects to the transmitted-side duct, concentrates at the duct wall between S_3 and S_2 in Fig. 8(a), between S_2 and S_1 in Fig. 8(b), and just in front of S_1 in Fig. 8(c). It can be said that the main reflection of the incident wave occurs at just in front of the slit that is dominant for resonance.

On the other hand, the conditions of the lower and higher resonances in Fig. 5(b) are shown in Figs. 8(d) and (e), each of which resembles Figs. 8(b) and (c), respectively. By comparison of the fields of Figs. 8(c) and (e), however, the level in the slit apparently differs from each other, i.e., both S_1 and S_2 seem dominant for (e) but the only S_1 for (c). It is reasonable to suppose that the effect of each adjoining slit is not separable when each resonant frequency of each slit comes close to each other.

4.2. *Single slit eccentric to the duct*

Fig. 9 shows a single eccentric slit treated here. Since the duct diameter is fixed at 41.3 mm in this paper, an eccentric slit can be defined by its diameter d, length l and eccentricity e. As the incident wave is limited to the plane wave, the eccentric direction is not required to specify. This type of slit was composed in the apparatus in Fig. 1 with the steel ring having a circular hole with specific d, l and e.

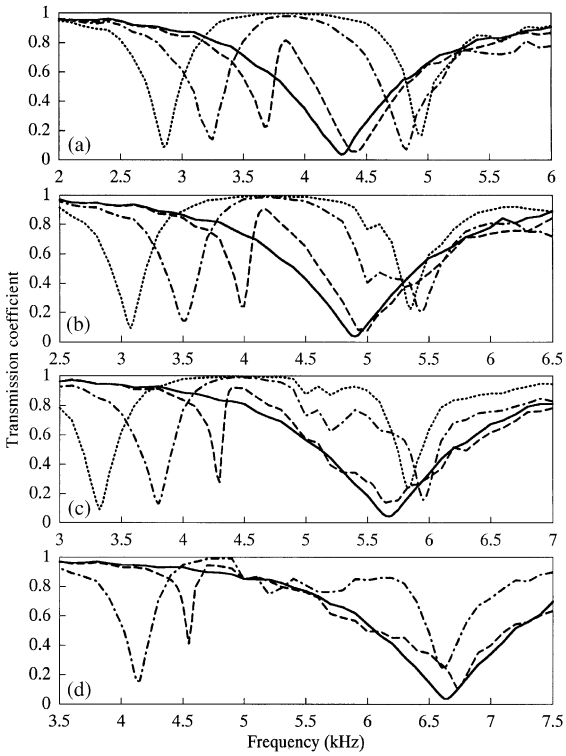

Fig. 10. Measured transmission coefficient at the single eccentric slit, $D = 41.3$ mm, $l = 5$ mm: (a) $d = 72$ mm; (b) $d = 68$ mm; (c) $d = 64$ mm; (d) $d = 60$ mm; ——, $e = 0$ mm; – – –, $e = 2$ mm; – – –, $e = 6$ mm; - - - - -, $e = 10$ mm.

Measured results of the eccentric slit of $l = 5$ mm, $d = 60$, 64, 68 or 72 mm and $e = 0$, 2, 6 or 10 mm are shown in Fig. 10, where lines are used instead of marks for legibility. Each line connects measured values obtained at the interval of 0.1 kHz in all the frequency range except near each minimum and maximum of the curves with 0.025 kHz resolution.

Since the slit is not axisymmetric to the duct axis, asymmetric sound modes can be radiated by reflection and transmission at the slit even if the incident wave is the plane wave alone. In the frequency range above 4.92 kHz that is the (1,0) cut-off at 25°C in the duct, therefore, the lowest asymmetric (1,0) mode wave can propagate in the duct. In our experimental method described in Section 2, however, transmission properties of the (1,0) mode wave in the duct cannot be evaluated. In Fig. 10, hence, the transmission coefficient indicates the amplitude ratio between the transmitted plane wave and the incident one. Even so, by our estimation traversing the microphone to the radial direction, the influence of the (1,0) mode on the transmitted-side sound field is not much serious within the configurations of slit treated here except the narrow frequency range close to the cut-off.

In every curve in Fig. 10, it is obvious that two minimums are observed except in the cases of $e = 0$. The sound field conditions at the lower and higher frequencies of these two minimums are termed the first and second resonance, respectively, for convenience' sake. To clarify both of the

resonant conditions, each resonant frequency collected in Fig. 10 is plotted in Fig. 11, where other results for $e = 1$, 4 and 8 mm obtained by the same manner as Fig. 10 are added.

In Fig. 11, the first resonant frequencies have a clear tendency to decrease at an almost constant rate as the eccentricity e increases and the slit diameter d increases. On the other hand, the second ones do not have such a tendency, and each value of them is not much different from the value of the corresponding concentric slit ($e = 0$).

In order to consider these resonant phenomena, FDM calculations were carried out. For confirming the reliability of the calculation, the transmission coefficient was evaluated by the amplitude ratio of sound pressure at the duct axis calculated by the FDM as shown in Fig. 12. In this figure, it is obvious that two minimums are observed except in the case of $e = 0$ and the frequencies of them are in good accordance with the measured ones in Fig. 11.

Fig. 13 shows calculated distributions of sound pressure level in cross-sections BB′ and AA′ in Fig. 2 at each resonant frequency in Fig. 12. Although the frequency is lower than the (1,0) cut-off in the duct (4.92 kHz) in all figures, an influence of the (1,0) mode observed in the transmitted-side duct becomes larger as the frequency comes closer to the cut-off. In an actual sound field, this non-propagating mode should decay more rapidly following an exponential curve.

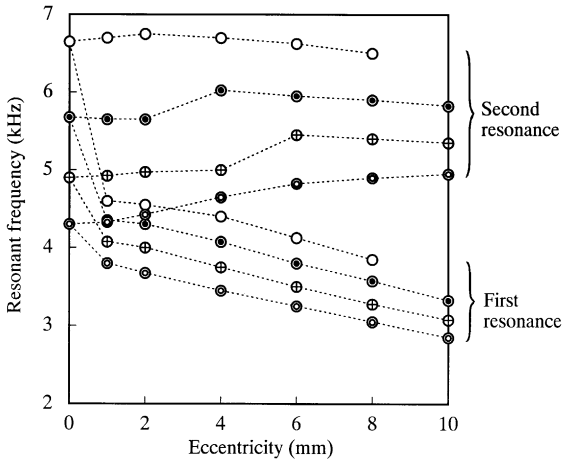

Fig. 11. Resonant frequency versus eccentricity of the single eccentric slit, $D = 41.3$ mm, $l = 5$ mm: ○, $d = 60$ mm; ◉, $d = 64$ mm; ⊕, $d = 68$ mm; ◎, $d = 72$ mm.

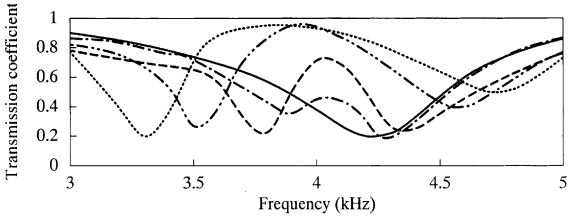

Fig. 12. Calculated transmission coefficient at the single eccentric slit by FDM, $D = 41.3$ mm, $l = 5$ mm, $d = 72$ mm: ——, $e = 0$ mm; – – –, $e = 1$ mm; – – –, $e = 2$ mm; – – – –, $e = 4$ mm; - - - - -, $e = 6$ mm.

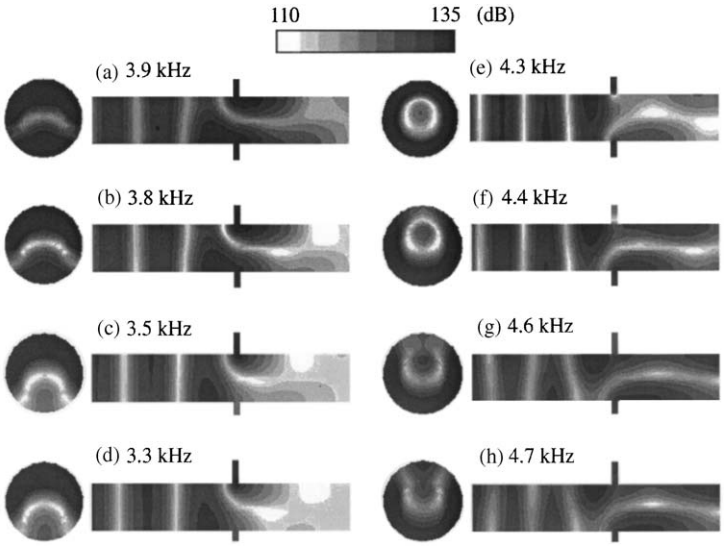

Fig. 13. Distribution of sound pressure level in the duct with the single eccentric slit, $D = 41.3$ mm, $l = 5$ mm, $d = 72$ mm: (a) and (e) $e = 1$ mm; (b) and (f) $e = 2$ mm; (c) and (g) $e = 4$ mm; (d) and (h) $e = 6$ mm; (a)–(d) at the first resonance; (e)–(h) at the second resonance.

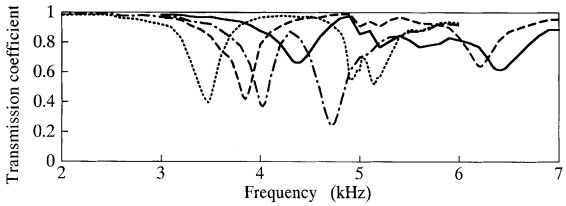

Fig. 14. Measured transmission coefficient at the single eccentric slit, $D = 41.3$ mm, $l = 2$ mm: ——, $d = 64$ mm, $e = 4$ mm; – – –, $d = 64$ mm, $e = 8$ mm; – – –, $d = 72$ mm, $e = 2$ mm; - - - - -, $d = 72$ mm, $e = 6$ mm.

As seen in each circle in Fig. 13 where the slit is eccentric to the upper direction, it can be said that the upper side of the slit becomes a dominant region for the first resonance (a–d) and the lower side for the second (e–h). In another viewpoint, however, the following interpretation can also be possible as seen in the cases of $e = 1$ and 2 mm. The node of sound appears rather horizontally for the first resonance (a and b) and circumferentially for the second (e and f), in other words, the sound field resembles the (1,0) mode's one for the first resonance and the concentric slit's one for the second. These sound pressure distributions give a good suggestion to understand the frequencies in Fig. 11, in which each second resonant frequency is not much different from the resonant frequency of the corresponding concentric slit ($e = 0$), but the first resonant frequency seems to have no relation to them and considerably lower than them.

As mentioned in Section 4.1, a shorter slit length causes a more insufficient resonance in a slit. In addition, an eccentric configuration seems to be disadvantage for its resonance against a concentric one. For reference, some measured results are shown in Fig. 14 for the eccentric slit of

$l = 2$ mm, using lines drawn by the same manner as Fig. 10. Judging from the curves in this figure compared with the ones of $l = 5$ mm in Fig. 10, it should be noted that an excessive short length is not favourable for using an eccentric slit as a muffler.

4.3. Serialized slits eccentric to the duct

From the results in Sections 4.1 and 4.2, it is expected that a more effective muffler might be composed by a mixture of these two configurations, i.e., by locating some eccentric slits in series in a duct. Although a large number of combinations of each slit having arbitrary size and eccentric direction can be considered, it is impossible to treat many of them in a limited space. Some results introduced here were obtained with limited parameters determined by referring to the conditions in Sections 4.1 and 4.2: the duct diameter $D = 41.3$ mm; the number of slits is three; each slit has the same diameter $d = 72$ mm, the same length $l = 5$ mm and the same interval $w = 1$ mm; the eccentric directions of them are on an identical diametral line. The formation of the slits treated here is realized in Fig. 4, giving the slits S_1, S_2 and S_3 the eccentricities e_1, e_2 and e_3, respectively, as shown in Fig. 9.

Fig. 15 shows transmission properties of serialized eccentric slits obtained by the experiment and calculation. In the value of the eccentricity noted in the legend of this figure, minus means that the corresponding slit shifts the opposite direction against the others, i.e., in Fig. 15(a), each

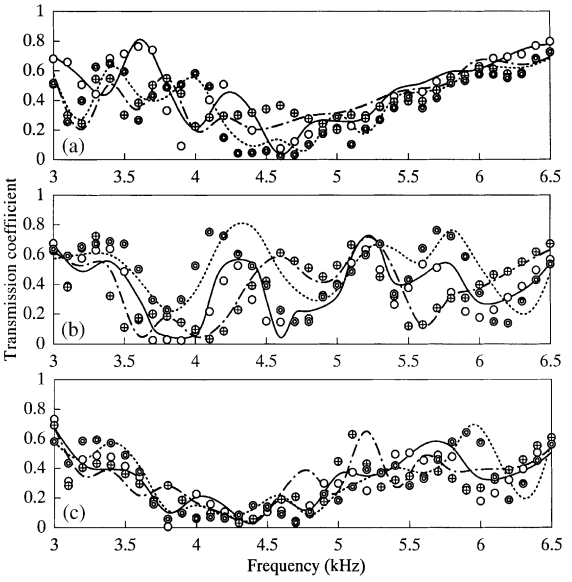

Fig. 15. Transmission coefficient at the serialized eccentric slits, $D = 41.3$ mm, $l = 5$ mm, $w = 1$ mm, $d_1 = d_2 = d_3 = 72$ mm: circular mark, measured; curved line, calculated by FDM: (a) ○, ——, $e_1 = 0$ mm, $e_2 = 2$ mm and $e_3 = 4$ mm; ⊕, – · –, $e_1 = 2$ mm, $e_2 = 4$ mm and $e_3 = 6$ mm; ◎, - - - - -, $e_1 = 0$ mm, $e_2 = 4$ mm and $e_3 = 6$ mm: (b) ○, ——, $e_1 = 2$ mm, $e_2 = -4$ mm and $e_3 = 6$ mm; ⊕, – – –, $e_1 = 4$ mm, $e_2 = -2$ mm and $e_3 = 6$ mm; ◎, - - - - -, $e_1 = 4$ mm, $e_2 = -6$ mm and $e_3 = 2$ mm: (c) ○, ——, $e_1 = 2$ mm, $e_2 = 4$ mm and $e_3 = -6$ mm; ⊕, – – –, $e_1 = 4$ mm, $e_2 = 2$ mm and $e_3 = -6$ mm; ◎, - - - - -, $e_1 = 2$ mm, $e_2 = 6$ mm and $e_3 = -4$ mm.

of three slits shifts to the same direction; in Fig. 15(b), only the middle slit S_2 shifts to the opposite direction against the other two slits; and in Fig. 15(c), the last slit S_3 does the same.

In Fig. 15, the variation of each curve of transmission coefficient shows more intricate appearance than the ones in Figs. 5 and 10. Nevertheless, the accordance between the measured and calculated results is good enough. The FDM calculation formulated in this research in a three-dimensional sound field is still reliable for such complicated problems.

In a sense, the property in Fig. 15(a) is expected to be the combined one of the properties in Figs. 5 and 10(a). In the lower frequency range (lower than about 4.5 kHz), however, the transmission coefficient is not suppressed enough against the expectation. In Fig. 15(b), the situation becomes worse for sound reduction, because several transmissive frequency bands appear. On the other hand, the property in Fig. 15(c) looks better than the other cases, i.e., the transmission coefficient is suppressed in a certain frequency range around the resonant frequency of the single concentric slit of $d = 72$ mm (about 4.3 kHz).

As an example, distributions of sound pressure level are shown in Fig. 16, in the condition that the configuration of slits is fixed at the second case of Fig. 15(a) and the frequency is varied. In each contour map, a node appears near the slit, and the position of it changes variously as the frequency changes. It is supposed that many types of resonant condition are likely to occur in such complicated sound fields. It has to be said that, hence, it is difficult to find a simple rule to predict the performance of such complicated combination of slits against relatively simple cases in Sections 4.1 and 4.2. Anyway, since the accuracy of the calculation is reliable, it may be possible

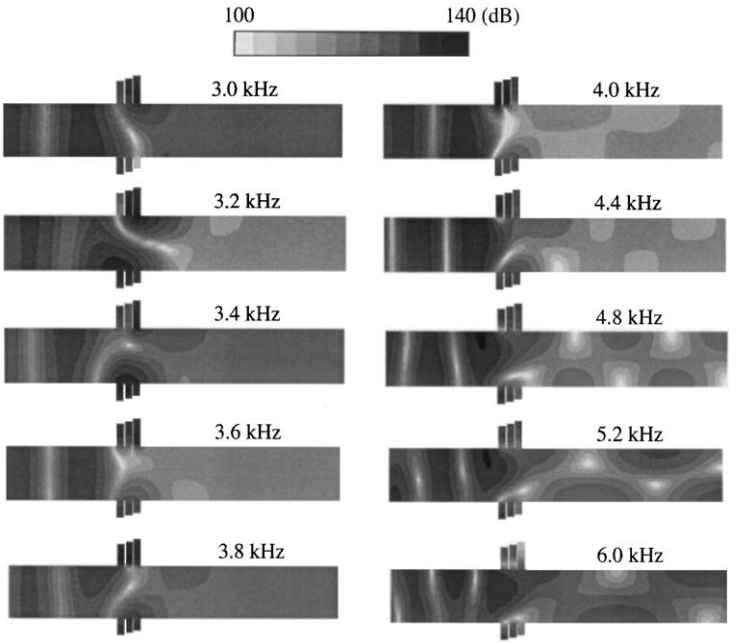

Fig. 16. Distribution of sound pressure level in the duct with the serialized eccentric slits, $D = 41.3$ mm, $l = 5$ mm, $w = 1$ mm, $d_1 = d_2 = d_3 = 72$ mm, $e_1 = 2$ mm, $e_2 = 4$ mm and $e_3 = 6$ mm.

to find out more effective configuration of slits for sound reduction using the calculation method in this paper.

5. Conclusions

In this paper, properties of slit-like expansion chambers, termed 'slit' here, in a duct were studied adding some modifications to their configuration. The performance of several types of slits as a sound attenuator was analysed by the experiment and calculation. The results obtained here are as follows:

(i) A numerical calculation using finite difference scheme was developed for a three-dimensional sound field in an arbitrary co-ordinate system. The accuracy of this calculation was confirmed by comparing with measured results obtained in a circular duct with several types of slits.

(ii) When three slits concentric to the duct and having different diameters from each other are placed in series in the duct, a summative property of each slit individually placed in the duct is basically obtained. When the resonant frequency of each slit comes close to each other in a certain range, however, an interaction among these slits occurs. In this situation, the effective frequency range becomes narrower against expectation, but the sound reduction level becomes sufficient in this frequency range.

(iii) When a single slit eccentric to the duct is placed, two resonant frequencies are obtained. The first frequency of them is apparently lower than the resonant frequency of the corresponding concentric slit, and the sound distribution in the slit at this frequency relatively resembles the (1,0) mode's one. On the other hand, the second frequency is comparatively close to the corresponding concentric slit's one.

(iv) When three slits eccentric to the duct are placed in series, the property becomes rather complicated, because many types of resonant condition could be occurred in various frequencies. Under the condition that each slit has the same size and shifts in an identical diametral line, a good performance for sound reduction is obtained in the case that the eccentric direction of the end slit is opposite against the others.

Acknowledgements

A portion of this research was supported by 'Japan Society for the Promotion of Science' through 'Grant-in-Aid for Encouragement of Young Scientists (No. 10750132)'.

References

[1] A.I. El-Sharkawy, A.H. Nayfeh, Effect of an expansion chamber on the propagation of sound in circular ducts, *Journal of the Acoustical Society of America* 63 (1978) 667–674.

[2] J. Ih, B. Lee, Analysis of higher-order mode effects in the circular expansion chamber with mean flow, *Journal of the Acoustical Society of America* 77 (1985) 1377–1388.

[3] A. Selamet, P.M. Radavich, The effect of length on the acoustic attenuation performance of concentric expansion chambers: an analytical, computational and experimental investigation, *Journal of Sound and Vibration* 201 (1997) 407–426.
[4] A. Sadamoto, Y. Murakami, Resonant properties of short expansion chambers in a circular duct: including extremely short cases and asymmetric mode wave incidence cases, *Journal of Sound and Vibration* 249 (2002) 165–187 doi:10.1006/jsvi.2001.3857.
[5] A. Sadamoto, Y. Murakami, Reduction of discrete-frequency fan noise using slit-like expansion chambers, *International Journal of Rotating Machinery* 9 (2003) 239–246.
[6] A. Selamet, Z.L. Ji, Acoustic attenuation performance of circular expansion chambers with offset inlet/outlet: I: analytical approach, *Journal of Sound and Vibration* 213 (1998) 601–617.
[7] A. Selamet, Z.L. Ji, Acoustic attenuation performance of circular expansion chambers with offset inlet/outlet: II. Comparison with experimental and computational studies, *Journal of Sound and Vibration* 213 (1998) 619–641.
[8] J.C. Tannehill, D.A. Anderson, R.H. Pletcher, *Computational Fluid Mechanics and Heat Transfer*, 2nd Edition, Taylor & Francis, Washington, DC, 1997.
[9] W. Kollmann, *Computational Fluid Dynamics*, Hemisphere, Washington, DC, 1980.
[10] D. Gottlieb, E. Turkel, Dissipative two-four method for time dependent problems, *Mathematics of Computation* 30 (1976) 703–723.
[11] R. Hixon, On increasing the accuracy of MacCormack schemes for aeroacoustic applications, AIAA Paper 97-1586, 1997, pp. 29–39.